J. Opt. A: Pure Appl. Opt. **11** (2009) 125411 (11pp) doi:10.1088/1464-4258/11/12/125411

Image hiding based on time-averaged fringes produced by non-harmonic oscillations

M Ragulskis[1], A Aleksa[1] and Z Navickas[2]

[1] Research Group for Mathematical and Numerical Analysis of Dynamical Systems, Kaunas University of Technology, Studentu 50-222, Kaunas LT-51368, Lithuania
[2] Department of Applied Mathematics, Kaunas University of Technology, Studentu 50-325B, Kaunas LT-51368, Lithuania

E-mail: minvydas.ragulskis@ktu.lt, algiment.aleksa@ktu.lt and zenonas.navickas@ktu.lt

Received 30 June 2009, accepted for publication 8 September 2009
Published 30 September 2009
Online at stacks.iop.org/JOptA/11/125411

Abstract
Image hiding based on time-averaged fringes produced by non-harmonic oscillations is presented in this paper. The secret image is embedded into the background moiré grating. Phase matching and initial stochastic phase deflection algorithms are used to encrypt the image. The decoding of the image is completely visual. The secret embedded image appears when the encrypted image is oscillated according to a predefined law of motion. No secret is leaked when the encrypted image is oscillated harmonically. Numerical experiments are used to illustrate the functionality of the method.

Keywords: visual cryptography, geometric moiré, interference fringes, time averaging, Bessel functions

1. Introduction

Visual cryptography is a cryptographic technique which allows visual information (pictures, text, etc) to be encrypted in such a way that the decryption can be performed by the human visual system, without the aid of computers. Visual cryptography was pioneered by Naor and Shamir in 1994 [1]. They demonstrated a visual secret sharing scheme, where an image was broken up into n shares so that only someone with all n shares could decrypt the image, while any $n-1$ shares revealed no information about the original image. Each share was printed on a separate transparency, and decryption was performed by overlaying the shares. When all n shares were overlaid, the original image would appear.

Since 1994, many advances in visual cryptography have been done. An efficient visual secret sharing scheme for color images is proposed in [2]. Halftone visual cryptography based on the blue noise dithering principles is proposed in [3]. Basis-matrices-free image encryption by random grids is developed in [4]. A generic method that converts a visual cryptography scheme into another visual cryptography scheme that has a property of cheating prevention is implemented in [5]. Colored visual cryptography without color darkening is developed in [6]. Secret sharing schemes based on Boolean operations without pixel expansion are proposed in [7]. Visual cryptography and polynomial-style sharing are combined in one image sharing method [8]. Sharing ability in visual cryptography up to any general number of multiple secrets in two circle shares is proposed in [9, 10]. A circular visual cryptography scheme for hiding multiple secret images is developed in [11]. Prioritization of the different pixel expansions for image contrast enhancement is proposed in [12]. Extended visual secret sharing schemes have been used to improve the quality of the shadow image in [13]. A new progressive image sharing technique is developed in [14]. Data hiding in halftone images using a conjugate ordered dithering algorithm is presented in [15]. A multi-ringed visual cryptography technique to hide secret messages on cylindrical surfaces of shares is proposed in [16].

Geometric moiré [17, 18] is a classical in-plane whole-field non-destructive optical experimental technique based on analysis of visual patterns produced by superposition of two regular gratings that geometrically interfere. Examples of gratings are equispaced parallel lines, concentric circles or arrays of dots. The gratings can be superposed by double-exposure photography, by reflection, by shadowing, or by

direct contact [19, 20]. Moiré patterns are used to measure variables such as displacements, rotations, curvature and strains throughout the viewed area. In-plane moiré is typically conducted with gratings of equispaced, parallel lines [18, 19].

Two basic goals exist in moiré pattern research. The first is the analysis of moiré patterns. The task is to analyze and characterize the distribution of moiré fringes in a moiré pattern. Most of the research in moiré pattern analysis deals with the interpretation of experimentally produced patterns of fringes and determination of displacements (or strains) at centerlines of appropriate moiré fringes. Moiré fringes in a pattern are enumerated using manual, semi-manual or fully automatic computational techniques [17].

Another goal is moiré pattern synthesis when the generation of a certain predefined moiré pattern is required. The synthesis process involves production of two such images that the required moiré pattern emerges when those images are superimposed [21]. Moiré synthesis and analysis are tightly linked and understanding one task gives insight into the other. Conditions ensuring that a desired moiré pattern will be present in the superposition of two images are predetermined; however, they do not specify these two original images uniquely. The freedom in choosing the superimposed images can be exploited to produce various degrees of visibility and ensure the desired properties. Several criteria are proposed in [22, 23] to resolve that freedom in moiré pattern synthesis.

Another technique based on optical moiré operations for image encryption and decryption is presented by simulation and experimentally in [24]. The moiré grating is generated by a computational algorithm as a harmonic function. The intensity of the reflectance map of the secret image is added as an argument of the harmonic moiré grating. The decryption is performed by overlapping the encrypted image with a key fringe pattern.

A technique based on optical operations on stochastic moiré patterns for image encryption and decryption is developed in [25]. In this method, an image is encrypted by a stochastic geometric moiré pattern deformed according to the image reflectance map. The decryption is performed using a pixel correlation algorithm in the encrypted image and the original stochastic geometrical moiré pattern.

The image hiding method based on time-averaging moiré is proposed in [26]. This method is based not on static superposition of moiré images, but on time-averaging geometric moiré. This method generates only one picture; the secret image can be interpreted by the naked eye only when the original encoded image is harmonically oscillated in a predefined direction at a strictly defined amplitude of oscillation. This method, strictly speaking, is not a visual cryptography scheme. It resembles a visual cryptography scheme because one needs a computer to encode a secret, and one can decode the secret without a computing device. Only one picture is generated, and the secret is leaked from this picture when parameters of the oscillation are appropriately tuned. In other words, the secret can be decoded by trial and error—if only one knows that he has to shake the slide. Therefore, additional image security measures are implemented in [26], particularly splitting of the encoded image into two shares. Oscillation of any of the shares separately does not reveal the secret. Two shares must be superimposed and then oscillated before the secret image can be interpreted.

The object of this paper is to develop such an image encoding method which would reveal the secret image not only at exactly tuned parameters of the oscillation, but would require that the time function determining the process of oscillation would comply with specific requirements. Moreover, the new method should not reveal the secret image at any amplitude of harmonic oscillations. Instead, the secret should be leaked only at carefully chosen parameters of this specific time function.

This paper is organized as follows. Initial definitions are given in section 2; main theorems are proven in section 3; the principles of image encryption are discussed in section 4; concluding remarks are given in section 5.

2. Initial definitions

Definition 1. Function $F(x)$ is a grayscale function if it is defined for all $x \in R$ and satisfies the following conditions:

- $0 \leqslant F(x) \leqslant 1$;
- has only a finite number of discontinuity points in every finite interval $[a, b]$; $a < b$.

It is assumed that 0 corresponds to the black color, 1 corresponds to the white color and all intermediate numerical values of a grayscale function correspond to an appropriate grayscale level.

Example 1. Functions $F_0(x) = 0$; $F_1(x) = 1$; $F_2(x) = \cos^2(x)$ are grayscale functions.

Definition 2. The time-averaging operator H_s is defined as [27]

$$H_s(x|F;\zeta_s) = \lim_{T\to\infty}\frac{1}{T}\int_0^T F(x-\zeta_s(t))\,\mathrm{d}t \qquad (1)$$

where t is time; T is the exposure time; $\zeta_s(t)$ is a function describing dynamic deflection from the state of equilibrium; s is a real parameter; $s \geqslant 0$; $x \in R$.

From this point forward we will assume that $\zeta_s(t)$ is a periodic function, its period being $2L$: $\zeta_s(t+2L) = \zeta_s(t)$; $L > 0$.

Corollary 1. *The condition of periodicity of $\zeta_s(t)$ yields*

$$H_s(x|F;\zeta_s) = \frac{1}{2L}\int_{a-L}^{a+L} F(x-\zeta_s(t))\,\mathrm{d}t \qquad (2)$$

where a is a fixed number; $a \in R$.

Example 2. If $\tilde{F}(x) = \frac{1}{2} + \frac{1}{2}\cos(\frac{2\pi}{\lambda}x)$ and $\tilde{\zeta}_s(x) = s\sin(\omega t + \varphi)$, where λ is the pitch of moiré grating, ω is

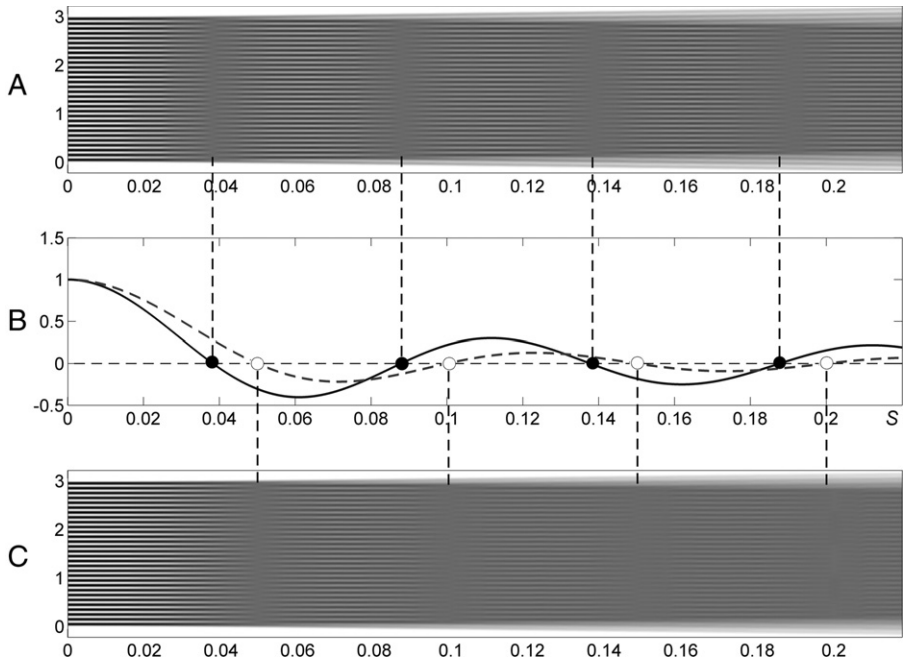

Figure 1. Patterns of time-averaged fringes produced by a harmonic moiré grating ($\lambda = 0.1$) oscillated harmonically (A) and by a 'zig-zag'-type time function (C). The line drawing in part (B) illustrates appropriate envelope functions and their roots; vertical dashed lines mark centerlines of corresponding time-averaged fringes.

the frequency of harmonic oscillations, φ is the phase and s represents the amplitude of harmonic oscillations, then

$$H_s\left(x|\tilde{F};\tilde{\zeta}_s\right) = \tfrac{1}{2} + \frac{1}{2}\cos\left(\frac{2\pi}{\lambda}x\right)\lim_{T\to\infty}\frac{1}{T}\int_0^T \cos\left(\frac{2\pi s}{\lambda}\sin(\omega t+\varphi)\right)\mathrm{d}t + \frac{1}{2}\sin\left(\frac{2\pi}{\lambda}x\right)\lim_{T\to\infty}\frac{1}{T}\int_0^T \sin\left(\frac{2\pi s}{\lambda}\sin(\omega t+\varphi)\right)\mathrm{d}t.$$

But $\lim_{T\to\infty}\frac{1}{T}\int_0^T \sin(\frac{2\pi s}{\lambda}\sin(\omega t+\varphi))\,\mathrm{d}t = \frac{1}{\pi}\int_{-\frac{\pi}{2}}^{\frac{\pi}{2}}\sin(\frac{2\pi s}{\lambda}\sin(t))\,\mathrm{d}t = 0$ due to the oddness of the sine function. Therefore

$$\begin{aligned} H_s\left(x|\tilde{F};\tilde{\zeta}_s\right) &= \frac{1}{2} + \frac{1}{2}\cos\left(\frac{2\pi}{\lambda}x\right)\lim_{T\to\infty}\frac{1}{T}\int_0^T \cos\left(\frac{2\pi s}{\lambda}\sin t\right)\mathrm{d}t \\ &\quad + \mathrm{i}\frac{1}{2}\cos\left(\frac{2\pi}{\lambda}x\right)\lim_{T\to\infty}\frac{1}{T}\int_0^T \sin\left(\frac{2\pi s}{\lambda}\sin t\right)\mathrm{d}t \\ &= \frac{1}{2} + \frac{1}{2}\cos\left(\frac{2\pi}{\lambda}x\right)J_0\left(\frac{2\pi s}{\lambda}\right) \end{aligned} \tag{3}$$

where $\mathrm{i}^2 = -1$; J_0 is a zero-order Bessel function of the first kind [28].

Equation (3) is a well-known result in experimental mechanics [17, 29] describing the formation of time-averaged moiré fringes. The envelope function modulating the original grayscale variation is $\frac{1}{2}\pm\frac{1}{2}J_0(\frac{2\pi s}{\lambda})$. Time-averaged fringes will form at such values of s where $J_0(\frac{2\pi s}{\lambda}) = 0$ (grayscale level at the center of a fringe is 0.5). The explicit relationship between the amplitude of harmonic oscillation, the pitch of the moiré grating and the order of a time-averaged fringe is

$$s_j = \frac{\lambda}{2\pi}r_j; \qquad j = 1, 2, \ldots \tag{4}$$

where j is the order of a time-averaged fringe which is determined using manual, semi-automatic or automatic fringe counting techniques [17], r_j is the jth root of the zero-order Bessel function of the first kind and s_j are the discrete values of the amplitude of harmonic oscillation.

The formation of time-averaged fringes for a one-dimensional harmonic grating is illustrated in figure 1(A) where the horizontal axis stands for the amplitude of harmonic oscillation s and a harmonic one-dimensional moiré grating $\tilde{F}(x) = \frac{1}{2} + \frac{1}{2}\cos(\frac{2\pi}{\lambda}x)$ is formed in the vertical direction. Time-averaged one-dimensional images are computed for every discrete value of s and visualized at appropriate abscissas. Time-averaged fringes can be interpreted by a naked eye; centers of fringes are located at geometric locations corresponding to roots of the zero-order Bessel function of the first kind (figure 1(B)).

3. Theoretical relationships

It is well known [30] that averaging in time produces the effect of blur caused by dynamic deflections of the registered object from the state of equilibrium. This blur can be characterized by the operation of algebraic convolution between the grayscale function (describing the static image at the state of equilibrium) and the point spread function (the density function of a random variable describing dynamic deflections from the state of equilibrium) [31].

From this point forward we assume that such a random variable ξ_s exists whose density function $p_s(x)$ satisfies the following requirements:

(i) $p_s(x) = 0$ when $|x| > s$ and $p_s(x) > 0$ when $|x| < s$; $s > 0$

(ii) $p_s(x) = p_s(-x)$ for all $x \in R$. (5)

(iii) $\mu_{2j} := E\xi^{2j} = \eta_{2j} \cdot s^{2j}$; $j = 0, 1, 2, \ldots$;

where $\eta_{2j} > 0$ and do not depend on s.

Corollary 2. *$E\xi_s^{2j+1} = 0$; $j = 0, 1, 2, \ldots$ (the average of an odd power of a random variable whose density function is a symmetric function equal to zero).*

The average of a function of the random variable ξ_s is

$$A := EF(x - \xi_s) = \int_{-\infty}^{+\infty} F(x - y)p_s(y)\,\mathrm{d}y = \int_{-s}^{s} F(x - y)p_s(y)\,\mathrm{d}y.$$

We denote $p_s(y)\,\mathrm{d}y := \mathrm{d}u$. Then $u = G_s(y) = \int_{-s}^{y} p_s(v)\,\mathrm{d}v$; $-s \leqslant y \leqslant s$. Moreover, the following statements hold:

(a) $G_s(y)$ is a strictly increasing function in interval $-s \leqslant y \leqslant s$.

(b) $G_s(-s) = 0$; $G_s(s) = 1$.

(c) The distribution function of the random variable ξ_s is

$$P(\xi_s < y) = \begin{cases} 0, & y < -s; \\ G_s(y), & -s \leqslant y \leqslant s; \\ 1, & y > s. \end{cases}$$

(d) An inverse function $y = G_s^{-1}(u)$ exists.

Thus, $A = \int_0^1 F(x - G_s^{-1}(u))\,\mathrm{d}u$. Variable change $t := 2Lu - L$ yields

$$EF(x - \xi_s) = \frac{1}{2L}\int_{-L}^{L} F\left(x - G_s^{-1}\left(\frac{t + L}{2L}\right)\right)\mathrm{d}t. \quad (6)$$

Definition 3. A time-averaging operator $H_s(x|F; \zeta_s(t))$ can be interpreted as a stochastic operator if there exists a random variable ξ_s whose density function $p_s(x)$ is such that $\zeta_s(t) = G_s^{-1}(\frac{t+L}{2L})$.

Corollary 3. *If $H_s(x|F; \zeta_s)$ can be interpreted as a stochastic operator, then $H_s(x|F; \zeta_s) = EF(x - \xi_s)$ (the proof follows from (6))*

Corollary 3 gives a physical interpretation of the process of averaging in time. The one-dimensional grayscale function is deflected from the state of equilibrium by a current realization of the stochastic variable ξ_s; the first-order mean is calculated over all possible realizations of ξ_s.

Corollary 4. *The following equalities hold true:*

$$H_s(x|F; \zeta_s) = \int_{-s}^{s} F(x \pm y)p_s(y)\,\mathrm{d}y := F(x) * p_s(x); \quad (7)$$

where the symbol $*$ stands for the algebraic operation of convolution.

Proof.

$$H_s(x|F; \zeta_s) = EF(x - \xi_s) = \int_{-\infty}^{+\infty} F(x - y)\,p_s(y)\,\mathrm{d}y = \int_{-s}^{s} F(x - y)p_s(y)\,\mathrm{d}y.$$

Let $y = -z$. Then, corollary 3 yields: $\int_{-s}^{s} F(x - y)p_s(y)\,\mathrm{d}y = -\int_{s}^{-s} F(x + z)p_s(-z)\,\mathrm{d}z = \int_{-s}^{s} F(x + z)p_s(z)\,\mathrm{d}z$, □

Example 3. Let us assume that the density function of a random variable $\tilde{\xi}_s$ is an arcsine density function:

$$\tilde{p}_s(x) = (1(x + s) - 1(x - s))\frac{1}{\pi\sqrt{s^2 - x^2}}; \quad (8)$$

where

$$1(v) = \begin{cases} 1, & \text{when } v \geqslant 0; \\ 0, & \text{when } v < 0 \end{cases}$$

is a unitary Heaviside function and μ_{2k} can be expressed in the following form:

$$\mu_{2k} = E\tilde{\xi}_s^{2k} = \frac{1}{\pi}\int_{-s}^{s} \frac{x^{2k}}{\sqrt{s^2 - x^2}}\,\mathrm{d}x = \frac{1}{\pi}\int_{-\frac{\pi}{2}}^{\frac{\pi}{2}} \frac{s^{2k}(\sin t)^{2k}}{s\cos t} s\cos t\,\mathrm{d}t = \frac{2}{\pi}s^{2k}\frac{(2k-1)!!}{(2k)!!}\frac{\pi}{2} = \frac{(2k-1)!!}{(2k)!!}s^{2k};$$

where $(2k-1)!! = 1\cdot 3\cdot\ldots\cdot(2k-1)$; $(2k)!! = 2\cdot 4\cdot\ldots\cdot(2k)$; $k = 1, 2, \ldots$.

On the other hand, $u = \int_{-s}^{y} \frac{1}{\pi\sqrt{s^2 - v^2}}\,\mathrm{d}v = \frac{1}{\pi}(\arcsin\frac{y}{s} + \frac{\pi}{2}) = G(y)$. Thus, $y = G^{-1}(u) = s \cdot \sin(\pi(u - \frac{1}{2}))$. Therefore

$$EF(x - \xi_s) = \int_{-s}^{s} F(x - y)\frac{1}{\pi\sqrt{s^2 - y^2}}\,\mathrm{d}y = \int_0^1 F\left(x - s\cdot\sin\left(\pi\left(u - \tfrac{1}{2}\right)\right)\right)\mathrm{d}u = \frac{1}{\pi}\int_{-\frac{\pi}{2}}^{\frac{\pi}{2}} F(x - s\cdot\sin t)\,\mathrm{d}t;$$

where $\pi(u - \frac{1}{2}) := t$. Thus, finally $\tilde{\zeta}_s(t) = s \cdot \sin t$ [32].

Example 4. Let us assume that the density function of a random variable $\bar{\xi}_s$ is an uniform density function: $\bar{p}_s(x) = (1(x + s) - 1(x - s))\frac{1}{2s}$; $E\bar{\xi}_s^{2k} = \frac{1}{2k+1}s^{2k}$.

Then, analogously to example 3:

$$\int_{-s}^{s} F(x - y)\frac{1}{2s}\,\mathrm{d}y = \int_0^1 F(x - s(2u - 1))\,\mathrm{d}u = \frac{1}{2L}\int_{-L}^{L} F\left(x - \frac{st}{L}\right)\mathrm{d}t.$$

Therefore $\bar{\zeta}_s(t) = \frac{s}{L}t$.

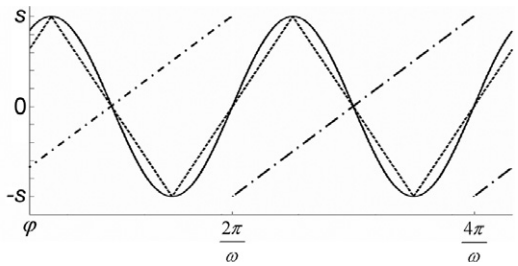

Figure 2. Periodic time functions at the same value of s: the solid line stands for the harmonic oscillation; dashed lines for the 'zig-zag'-type time function, and dashed–dotted lines for the 'saw' type time function.

In fact, many different periodic functions yield $G(y) = \int_{-s}^{y} \frac{1}{2s}\,\mathrm{d}v = \frac{y+s}{2s}$. Typical examples are 'zig-zag'-and 'saw'-type functions (figure 2):

$$\hat{\zeta}_s(t) = \begin{cases} \dfrac{2s\omega}{\pi}\left(t - \left(-\dfrac{\pi}{2\omega} - \varphi + \dfrac{2\pi}{\omega}k\right)\right) - s \\ \text{when } \left(-\dfrac{\pi}{2\omega} - \varphi + \dfrac{2\pi}{\omega}k\right) \leqslant t \leqslant \left(\dfrac{\pi}{2\omega} - \varphi + \dfrac{2\pi}{\omega}k\right) \\ -\dfrac{2s\omega}{\pi}\left(t - \left(\dfrac{\pi}{2\omega} - \varphi + \dfrac{2\pi}{\omega}k\right)\right) + s \\ \text{when } \left(\dfrac{\pi}{2\omega} - \varphi + \dfrac{2\pi}{\omega}k\right) \leqslant t \leqslant \left(\dfrac{3\pi}{2\omega} - \varphi + \dfrac{2\pi}{\omega}k\right) \end{cases} \tag{9}$$

$$\bar{\zeta}_s(t) = \frac{s\omega}{\pi}\left(t - \varphi + \frac{2\pi}{\omega}k\right) \quad \text{when } \left(-\frac{\pi}{\omega} - \varphi + \frac{2\pi}{\omega}k\right) \leqslant t < \left(\frac{\pi}{\omega} - \varphi + \frac{2\pi}{\omega}k\right) \quad k = 0, \pm 1, \pm 2, \ldots. \tag{10}$$

It can be noted that density functions $\tilde{p}_s(x)$ and $\bar{p}_s(x)$ do not depend on ω. This is a well-known effect in experimental mechanics that the frequency of harmonic oscillations does not have any influence on the formation of time-averaged fringes (see (3)) [17].

Theorem 1. *Let* $F(x) = \sum_{k=0}^{+\infty} a_k \frac{x^k}{k!}$*; for all* x *and given* $a_k \in R$*. Then*

$$H_s(x|F;\zeta_s) = \sum_{j=0}^{+\infty} \left(D_x^{2j} F(x)\right) \frac{\mu_{2j}}{(2j)!} \tag{11}$$

where D_x^n *is the operator of differentiation (*x *is the variable of differentiation,* n *is the order of differentiation) and* $s \geqslant 0$*.*

Proof. The following identities are exploited in this proof:

(a) $\sum_{l=0}^{+\infty} a_{l+2j} \frac{x^l}{l!} = D_x^{2j}\left(\sum_{l=0}^{+\infty} a_l \frac{x^l}{l!}\right)$

(b) $\frac{1}{(-n)!} = 0$ for $n = 1, 2, \ldots$.

$$H_s(x|F;\zeta_s) = \int_{-s}^{s} \sum_{k=0}^{+\infty} a_k \frac{(x+y)^k}{k!} p_s(y)\,\mathrm{d}y = \sum_{k=0}^{+\infty} \frac{a_k}{k!} \sum_{0}^{k} \binom{k}{j} x^{k-j} \int_{-s}^{s} y^j p_s(y)\,\mathrm{d}y = \sum_{k=0}^{+\infty}\sum_{j=0}^{+\infty} \frac{a_k}{k!} \frac{k! x^{k-j}}{(k-j)!\,j!}\mu_j = \sum_{k=0}^{+\infty}\sum_{r=0}^{+\infty} a_k \frac{x^{k-2r}}{(k-2r)!(2r)!}\mu_{2r}$$

because $\mu_{2r+1} = 0$, $r = 0, 1, 2, \ldots$. The last equality holds since $\int_{-s}^{s} y^{2r+1} p_s(y)\,\mathrm{d}y = 0$, ($p_s(y)$ is an even function).

The notation $k - 2r = l$ yields

$$H_s(x|F;\zeta_s) = \sum_{r=0}^{+\infty} \left(\sum_{k=l}^{+\infty} a_{l+2r} \frac{x^l}{l!}\right) \frac{\mu_{2r}}{(2r)!} = \sum_{r=0}^{+\infty} \left(D_x^{2r} F(x)\right) \frac{\mu_{2r}}{(2r)!}.$$

□

Example 5. Harmonic oscillations yield $\mu_{2j} = \frac{(2j-1)!!}{(2j)!!} s^{2j}$ (example 3). Then

$$\frac{\mu_{2j}}{(2j)!} = \frac{(2j-1)!!}{(2j)!!(2j)!} s^{2j} = \frac{s^{2j}}{((2j)!!)^2} = \frac{s^{2j}}{(2^j j!)^2}$$

and

$$H_s(x|F;\tilde{\zeta}_s) = \sum_{j=0}^{+\infty} \left(D_x^{2j} F(x)\right) \frac{s^{2j}}{(2^j j!)^2}.$$

Corollary 5. *If* $D_x^{2j} F(x) = (-1)^j \omega^{2j} F(x)$*, then*

$$H_s(x|F;\zeta_s) = \sum_{j=0}^{+\infty} \left(D_x^{2j} F(x)\right) \frac{\mu_{2j}}{(2j)!} = \left(\sum_{j=0}^{+\infty} (-1)^j \eta_{2j} \frac{(\omega s)^{2j}}{(2j)!}\right) F(x), \tag{12}$$

though $F(x)$ *is not necessarily a grayscale function.*

Example 6. If $F(x) = c\exp(\pm \mathrm{i}\omega x)$; $c \in R$; $\mathrm{i}^2 = -1$, then

$$H_s(x|c\exp(\pm\mathrm{i}\omega x);\zeta_s) = c\exp(\pm\mathrm{i}\omega x) \sum_{j=0}^{+\infty} (-1)^j \eta_{2j} \frac{(\omega s)^{2j}}{(2j)!}. \tag{13}$$

Corollary 6. *The Fourier transform of the density function is*

$$\Phi p_s(x) = \int_{-\infty}^{+\infty} \exp(-\mathrm{i}x\Omega)\, p_s(x)\,\mathrm{d}x = \int_{-s}^{s} \exp(-\mathrm{i}x\Omega)\, p_s(x)\,\mathrm{d}x = \int_{-s}^{s} \sum_{j=0}^{+\infty} \frac{(-\mathrm{i}x\Omega)^{2j}}{(2j)!} p_s(x)\,\mathrm{d}x = \sum_{j=0}^{+\infty} \frac{(-1)^j \Omega^{2j}}{(2j)!} \int_{-s}^{s} x^{2j} p_s(x)\,\mathrm{d}x = \sum_{j=0}^{+\infty} (-1)^j \Omega^{2j} \mu_{2j} = \sum_{j=0}^{+\infty} (-1)^j \frac{\eta_{2j} s^{2j}}{(2j)!} \Omega^{2j} = P_s(\Omega) \tag{14}$$

where Φ *stands for the Fourier transform.*

Theorem 2. *$H_s(x|\exp(\mathrm{i}\omega x);\zeta_s) = \exp(\mathrm{i}\omega x)\cdot P_s(\omega)$ where $P_s(\Omega) = \Phi p_s(x) = \sum_{j=0}^{+\infty}(-1)^j\eta_{2j}\frac{(\Omega s)^2}{(2j)!}$.*

The proof follows from properties of the density function $p_s(x)$ and its Fourier transform $P_s(\Omega)$.

Corollary 7. *If a periodic grayscale function with a period $2L$ can be expanded into a Fourier series:*

$$\hat{F}(x) = \frac{a_0}{2} + \sum_{k=1}^{+\infty}\left(a_k\cos\frac{k\pi x}{L} + b_k\sin\frac{k\pi x}{L}\right); \quad a_k, b_k \in R, \tag{15}$$

then

$$H_s\left(x|\hat{F};\zeta_s\right) = \frac{a_0}{2} + \sum_{k=1}^{+\infty}\left(a_k\cos\frac{k\pi x}{L} + b_k\sin\frac{k\pi x}{L}\right)P_s\left(\frac{k\pi}{L}\right). \tag{16}$$

Corollary 8. *If $\tilde{\zeta}_s(t) = s\sin(\omega t+\varphi)$, then*

$$H_s(x|\hat{F};\tilde{\zeta}) = \frac{a_0}{2} + \sum_{k=1}^{+\infty}\left(a_k\cos\frac{k\pi x}{L} + b_k\sin\frac{k\pi x}{L}\right)J_0\left(\frac{k\pi}{L}s\right), \tag{17}$$

because now

$$\begin{aligned} P_s(\Omega) &= \int_{-\infty}^{+\infty}\tilde{p}_s(x)\mathrm{e}^{-\mathrm{i}x\Omega}\,\mathrm{d}x \\ &= \frac{2}{\pi}\sum_{k=0}^{+\infty}\frac{(-1)^k\,\Omega^{2k}}{(2k)!}\frac{(2k-1)!!}{(2k)!!}\frac{\pi}{2}s^{2k} \\ &= \sum_{k=0}^{+\infty}(-1)^k\frac{(\Omega s)^{2k}}{(2k!!)^2} = \sum_{k=0}^{+\infty}(-1)^k\left(\frac{1}{k!}\left(\frac{\Omega s}{2}\right)^k\right)^2 \\ &= J_0(\Omega s) \end{aligned} \tag{18}$$

and the arcsine density function satisfies requirements (i)–(iii) in (5) (compare to example 2). Moreover, it can be easily checked that $a_0 = 1$ in this case.

Corollary 9. *Analogously, if $\hat{\zeta}_s(t)$ is a 'zig-zag' function described by (9), then*

$$H_s(x|\hat{F};\hat{\zeta}_s) = \frac{a_0}{2} + \sum_{k=1}^{+\infty}\left(a_k\cos\frac{k\pi x}{L} + b_k\sin\frac{k\pi x}{L}\right)\frac{\sin\left(\frac{k\pi}{L}s\right)}{\left(\frac{k\pi}{L}s\right)}, \tag{19}$$

because in this case $P(\Omega) = \frac{\sin(\Omega s)}{\Omega s}$, and the uniform density function satisfies requirements (i)–(iii) in (5).

4. Image hiding based on time average moiré

4.1. Case when the grayscale function is a harmonic function

If the grayscale function is a harmonic function $\tilde{F}(x) = \frac{1}{2}+\frac{1}{2}\cos(\frac{2\pi}{\lambda}x)$, time-averaged fringes will form in both cases when the density function of dynamic deflections from the state of equilibrium is the arcsine density function or the uniform density function (figure 1). In the first case, corollary 8 yields $H_s(x|\tilde{F};\tilde{\zeta}_s) = \frac{1}{2}+\frac{1}{2}\cos(\frac{2\pi}{\lambda}x)J_0(\frac{2\pi}{\lambda}s)$ ($L = 0.5\lambda$; compare to example 1). Time-averaged fringes will form at such values of s where $J_0(\frac{2\pi}{\lambda}s) = 0$ (figure 1(A)). In other words, the time-averaged image will be evenly gray for all $x \in R$ when the amplitude of harmonic oscillations is given by equation (3).

In the second case, corollary 9 yields $H_s(x|\tilde{F};\hat{\zeta}_s) = \frac{1}{2}+\frac{1}{2}\cos(\frac{2\pi}{\lambda}x)\frac{\sin(\frac{2\pi}{\lambda}s)}{(\frac{2\pi}{\lambda}s)}$. Now, the relationship between the amplitude of the 'zig-zag'-type oscillations (see (7)), the order of the time-averaged fringe and the pitch of the grating is

$$s_j = \frac{j\lambda}{2}; \qquad j = 1, 2, \ldots. \tag{20}$$

Differences between (4) and (20) are illustrated in figure 1(B).

4.2. Case when the grayscale function is a periodic but not a harmonic function

As mentioned previously, the image hiding technique based on time-averaging moiré and harmonic oscillations [26] may have problems with security of the secret image. One can try a trial-and-error method to leak the secret (of course, if one knows that he has to shake the slide). More complex encoding algorithms are used in [26] to overcome this drawback. The main object of this paper to construct such a secret image encoding method that harmonic oscillation of the slide would not leak the secret at any possible amplitude of oscillations.

First of all, we select a stepped moiré grating:

$$\hat{F}(x) = \begin{cases} 1, & \text{when } x \in \left[\lambda j; \frac{(1-s)\lambda}{2}+\lambda j\right] \\ & \cup\left[\frac{(1+s)\lambda}{2}+\lambda j; \lambda(j+1)\right] \\ 0, & \text{when } x \in \left(\frac{(1-s)\lambda}{2}+\lambda j; \frac{(1+s)\lambda}{2}+\lambda j\right) \end{cases} \tag{21}$$

where $j = 0, \pm1, \pm2, \ldots$ and the parameter s determines the ratio between the widths of white and black bands in a moiré grating (figure 3). The period of this grating is λ and $\hat{F}(x)$ can be expanded into a Fourier series. Coefficients of the expansion (see (15)) are

$$\hat{F}(x) = \begin{cases} a_0 = 2(1-s) \\ a_k = \dfrac{\sin(k\pi(1-s)) - \sin(k\pi(1+s))}{k\pi} \\ b_k = \dfrac{\cos(k\pi(1+s)) - \cos(k\pi(1-s))}{k\pi} \end{cases} \tag{22}$$

where $k = 1, 2, \ldots$.

A harmonic and a stepped moiré grating are illustrated in figure 3; numerical values of coefficients a_k and b_k are illustrated at $s = 0.5$ (when widths of white and black bands are equal).

If a stepped grayscale function is oscillated by a 'zig-zag' deflection function, the time-averaged image is defined by corollary 9: $H_s(x|\hat{F};\hat{\zeta}_s) = \frac{a_0}{2} + \sum_{k=1}^{+\infty}(a_k\cos\frac{k2\pi x}{\lambda} + b_k\sin\frac{k2\pi x}{\lambda})\frac{\sin(\frac{k2\pi}{\lambda}s)}{(\frac{k2\pi}{\lambda}s)}$. We assume that $\lambda = 0.1$ and select the first term of the sum at $k = 1$:

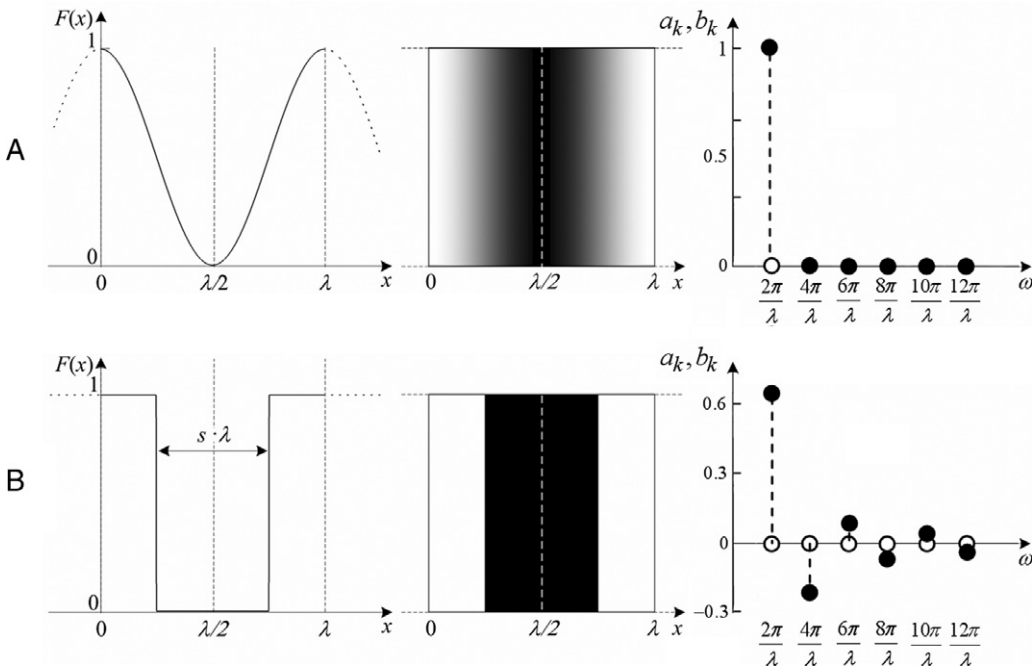

Figure 3. Harmonic (A) and stepped (B) moiré gratings. The left column illustrates one-dimensional grayscale functions; the middle column the corresponding grayscale levels and the right column the coefficients of Fourier expansion a_k (white circles) and b_k (black circles).

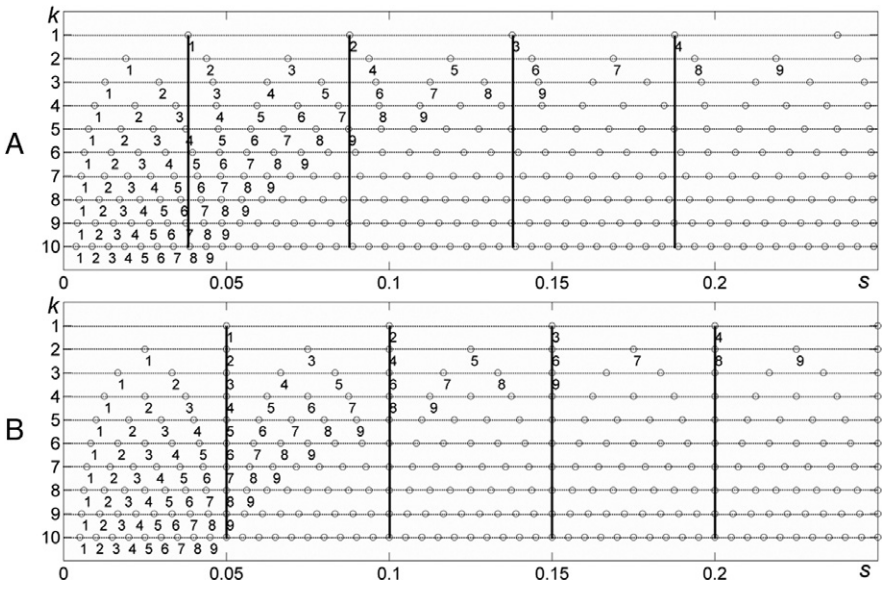

Figure 4. Distribution of centers of time-averaged fringes for different harmonic components of Fourier expansion of a moiré grating: harmonic oscillations (A); 'zig-zag'-type oscillations (B); only the first nine roots are numbered for clarity.

$(a_1 \cos\frac{2\pi x}{\lambda} + b_1 \sin\frac{2\pi x}{\lambda})\frac{\sin(\frac{2\pi}{\lambda}s)}{(\frac{2\pi}{\lambda}s)}$. This term turns to zero at $s_j = \frac{j\lambda}{2}$; $j = 1, 2, \ldots$. We visualize these values of s_j on the top dashed line (corresponding to $k = 1$) in figure 4(A). Analogously, we mark $s_j = \frac{j\lambda}{2k}$; $j = 1, 2, \ldots$ for other values of k in figure 4(A). It is clear that there exist such values of s where all terms of the infinite sum in (19) will turn to zero (these values of s are marked by solid vertical lines in figure 4(A)). In other words, time-averaged fringes will form at $s_j = \frac{j\lambda}{2}$; $j = 1, 2, \ldots$.

But if a stepped grayscale function is oscillated harmonically, the time-averaged image becomes $H_s(x|\hat{F}; \tilde{\zeta}) = \frac{a_0}{2} + \sum_{k=1}^{+\infty}(a_k \cos\frac{k2\pi x}{\lambda} + b_k \sin\frac{k2\pi x}{\lambda}) J_0(\frac{k2\pi}{\lambda}s)$ (corollary 8). Again, we mark values $s_j = \frac{\lambda r_j}{2\pi k}$; $j = 1, 2, \ldots$ where the kth term of the infinite sum in (17) turns to zero. But roots of the zero-order Bessel function of the first kind are distributed not regularly. Therefore, one cannot find any value of s where the infinite sum in (19) turns to zero (figure 4(B)). Thus, if the Fourier expansion of a moiré grating function comprises more than one harmonic component, no time-averaged fringes will

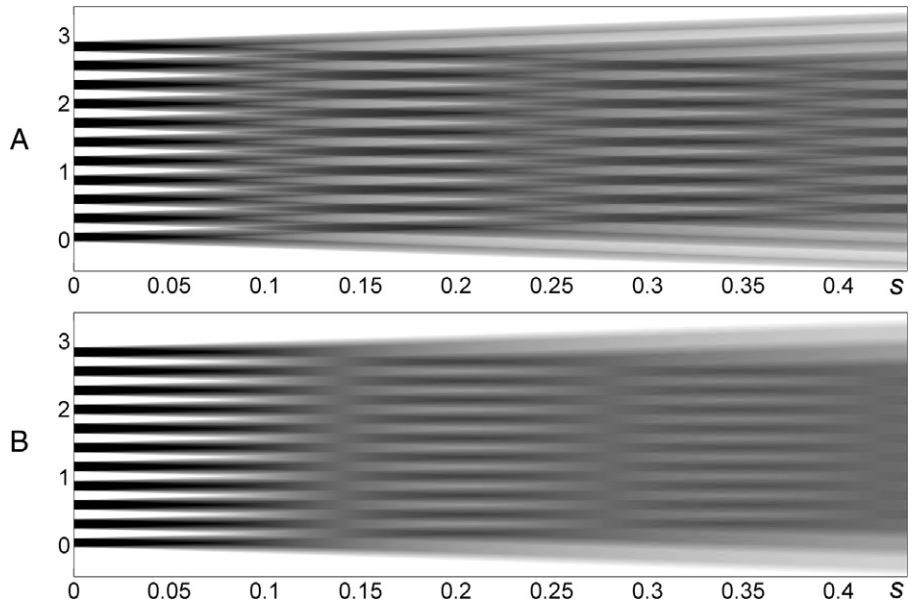

Figure 5. Time-averaged fringes produced by a stepped moiré grating ($\lambda = 0.286$) oscillated harmonically (A) and by a 'zig-zag'-type time function (B).

Figure 6. The secret image.

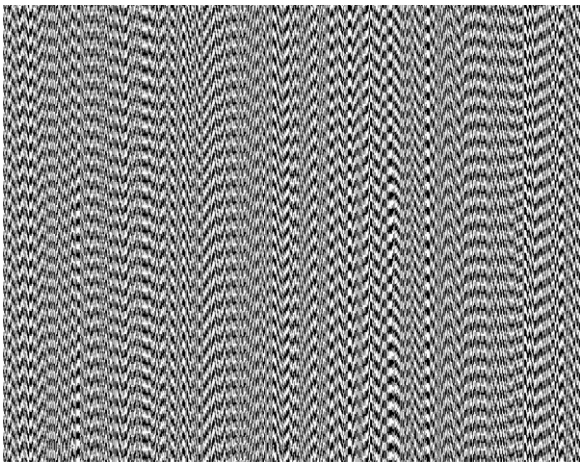

Figure 7. The secret image encoded into the background moiré grating. Pitch of the background moiré grating is $\lambda_0 = 1.7214$ mm; the pitch at zones inherent to the secret image is $\lambda_1 = 1.5649$ mm.

form in a time-averaged image of this moiré grating produced by harmonic oscillations. This is an important conclusion and it will be exploited in the construction of a new image hiding method.

We illustrate the above-mentioned effect in figure 5 where a stepped grayscale function is oscillated by a harmonic (figure 5(A)) and a 'zig-zag' deflection function (figure 5(B)). Time-averaged fringes are clearly seen in figure 5(B), but a complex 'zig-zag' type pattern is formed in figure 5(A) instead.

4.3. Image encoding into a moiré grating

Keeping the above-mentioned considerations in mind, we use stepped moiré gratings for image encoding. Otherwise, the encoding procedure is similar to the image hiding technique described in [26]. The secret image is shown in figure 6; the encoded image is shown in figure 7. We use phase matching and stochastic initial phase deflection algorithms to encode the secret into the background moiré pattern. These algorithms are described in detail in [26]; nevertheless, these algorithms are illustrated in figures 8 and 9 as the moiré grating used is different.

The digital image is constructed as a set of vertical columns of pixels (constitutive moiré grating lines are horizontal in our experiment). Every single vertical column corresponds to a one-dimensional set of pixels. The procedure of the image embedding into a moiré grating can be characterized by the following steps.

First of all the pitch of the background image λ_0 must be selected. We select that one pitch of the background image comprises 11 black pixels and 11 white pixels ($s = 0.5$). The size of the digital image in figure 7 is 80 mm $\times$ 48.2 mm. We use 28 pitches of the one-dimensional stepped grayscale function in the vertical column; thus $\lambda_0 = 1.7214$ mm. The

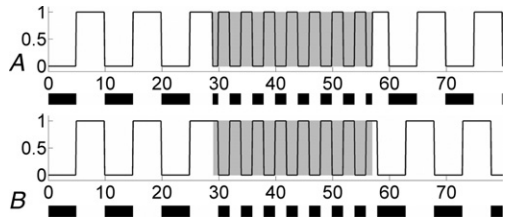

Figure 8. Graphical illustration of the phase matching algorithm at boundaries between the background and a zone inherent to the secret image (the shaded region): before the algorithm is applied (A) and after the algorithm is applied (B).

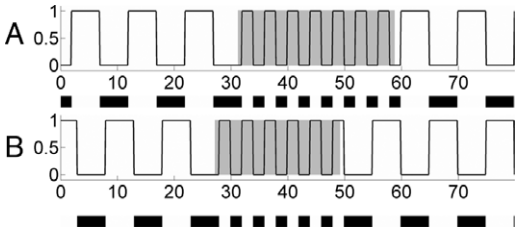

Figure 9. Graphical illustration of the stochastic initial phases deflection algorithm applied to two adjacent columns of pixels ((A) and (B)); shaded regions stand for zones inherent to the secret image.

next step is the selection of pitches of the encrypted image λ_1. We select that one pitch of the encrypted image comprises 10 black pixels and 10 white pixels ($\lambda_1 = 1.5649$ mm). Next we adapt the phase matching algorithm for the stepped grayscale function in order to avoid fragments of moiré grating at boundaries between the background and the encoded image as shown in figure 8 (vertical pixel lines are represented as horizontal lines to minimize the size of the figure). Finally, stochastic phase deflection at the top of adjacent vertical columns of pixels is performed. This procedure is illustrated in figure 9. Such random scrambling of initial phases may appear similar to the concept of stochastic geometric moiré presented in [25]. In fact, these two concepts are completely different—pixels of the background image are not shifted from their original locations in contrast to the technique exploited in [25].

4.4. Decoding of the secret image

The proposed method is a modification of the visual cryptography method. The decryption can be performed by the human visual system, without the aid of computers. It can be considered as a development of the image hiding method presented in [26]. The secret image cannot be leaked if the encoded image is oscillated harmonically. This statement holds for any amplitude of harmonic oscillations.

Visual decoding of the encoded image in figure 7 is performed when the image is oscillated around the state of equilibrium by a 'zig-zag' (see (9)) or a 'saw' function (see (10)). In fact, the only requirement is that the density function of the function describing dynamic deflections from the state of equilibrium is a symmetric uniform density

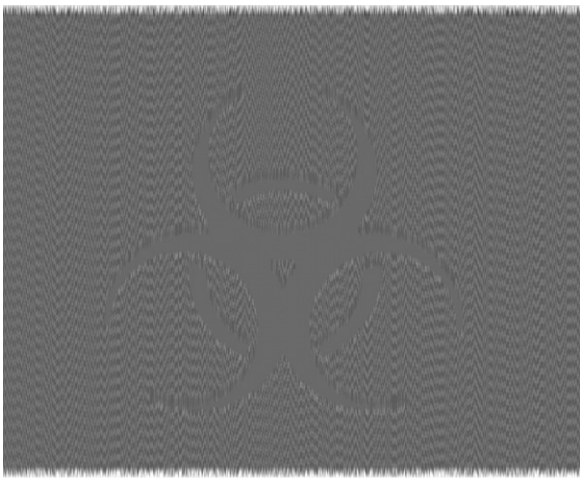

Figure 10. Computational visualization of the secret image when the encoded image is oscillated by a 'zig-zag'-type time function at $s = \frac{\lambda_1}{2} = 0.782\,45$ mm; time-averaged fringes are formed at zones inherent to the secret image.

Figure 11. Computational visualization of the secret image when the encoded image is oscillated by a 'zig-zag'-type time function at $s = \frac{\lambda_0}{2} = 0.860\,70$ mm; time-averaged fringes are formed at the background.

function (satisfying requirements of (5)). It must be noted that the secret image will not be leaked at any amplitude of the 'zig-zag' function; the parameter s in (9) must be equal to one of the specific values defined by equation (20).

In our case, the first time-averaged fringe will form at the region occupied by the secret image when $s = \frac{\lambda_1}{2} = 0.782\,45$ mm. The resulting image is illustrated in figure 10. It can be noted that a similar time-averaged images can be produced at higher discrete amplitudes $s_j = \frac{j\lambda_1}{2}$; $j = 2, 3, \ldots$. Alternatively, the secret image can be visualized when the time-averaged image is formed in the background at $s = \frac{\lambda_0}{2} = 0.860\,70$ mm. The resulting digital image is shown in figure 11; similar images can be produced at $s_j = \frac{j\lambda_0}{2}$; $j = 2, 3, \ldots$. But no secret image can be revealed when s does not coincide with the above-mentioned discrete values. Time-averaged image at $s = 0.8$ mm is shown in figure 12.

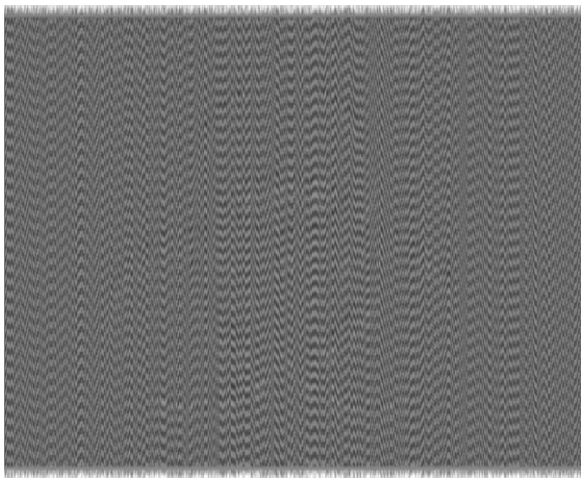

Figure 12. The secret image cannot be leaked when the amplitude of 'zig-zag'-type oscillations is not pre-selected accordingly; the time-averaged image is shown at $s = 0.8$ mm.

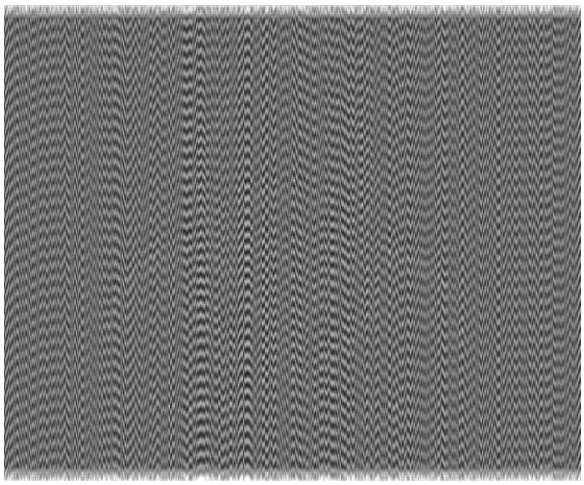

Figure 13. The secret image cannot be leaked when oscillations are harmonic; the time-averaged image is shown at $s = \frac{r_1\lambda_1}{2\pi} = 0.598\,94$ mm.

But the most important aspect of the presented encoding method is that the decoding cannot be produced by harmonic oscillations. The secret image will not be leaked at any amplitude of harmonic oscillations. The time-averaged image produced by harmonic oscillations at $s = \frac{r_1\lambda_1}{2\pi} = 0.598\,75$ is shown in figure 13.

5. Concluding remarks

A new image hiding method based on time-averaging moiré and non-harmonic oscillations is presented in this paper. We have demonstrated the functionality of the method using uniform density functions. The 'zig-zag' time function defined by equation (9) is probably one of the most convenient time functions which can be experimentally executed by a vibration excitation system (compared to other time functions whose density function is a symmetric uniform density function).

Anyway, this method can be extended for different density functions. A density function should satisfy requirements (i)–(iii) in (5) and be different from the arcsine density function. Then, appropriate manipulations with moiré gratings may enable visualization of secret embedded images only when the encoded image is oscillated by a corresponding law of motion. It can be noted that Gaussian density function is not applicable for this purpose—time-averaged moiré fringes are not generated by the Gaussian blur [33].

The security of the proposed image hiding method is much higher compared to the image hiding method based on time-averaging moiré and harmonic oscillations [26]. Anyway, one can use an additional image splitting technique into two (or n) shares [26] if even higher security of the encryption is required.

References

[1] Naor M and Shamir R 1994 Visual cryptography *Lect. Notes Comput. Sci.* **950** 1–12

[2] Shyu S H 2006 Efficient visual secret sharing scheme for color images *Pattern Recognit.* **39** 866–80

[3] Zhou Z, Arce G R and Di Crescenzo G 2006 Halftone visual cryptography *IEEE Trans. Image Process.* **15** 2441–53

[4] Shyu S H 2007 Image encryption by random grids *Pattern Recongnit.* **40** 1014–31

[5] Hu C M and Tzeng W G 2007 Cheating prevention in visual cryptography *IEEE Trans. Image Process.* **16** 36–45

[6] Cimato S, De Prisco R and De Santis A 2007 Colored visual cryptography without color darkening *Theor. Comput. Sci.* **374** 261–76

[7] Wang D S, Zhang L, Ma N and Li X 2007 Two secret sharing schemes based on Boolean operations *Pattern Recognit.* **40** 2776–85

[8] Lin S J and Ling J C 2007 VCPSS: a two-in-one two-decoding-options image sharing method combining visual cryptography (VC) and polynomial-style sharing (PSS) approaches *Pattern Recognit.* **40** 3652–66

[9] Shyu S J, Huang S Y, Lee Y K, Wang R Z and Chen K 2007 Sharing multiple secrets in visual cryptography *Pattern Recognit.* **40** 3633–51

[10] Feng J B, Wu H C, Tsa C S, Chang Y F and Chu Y P 2008 Visual secret sharing for multiple secrets *Pattern Recognit.* **41** 3572–81

[11] Hsu H C, Chen J, Chen T S and Lin Y H 2007 Special type of circular visual cryptography for multiple secret hiding *Imaging Sci. J.* **55** 175–9

[12] Yang C N and Chen T S 2007 Visual secret sharing scheme: prioritizing the secret pixels with different pixel expansions to enhance the image contrast *Opt. Eng.* **46** 097005

[13] Yang C N and Chen T S 2007 Extended visual secret sharing schemes: improving the shadow image quality *Int. J. Pattern Recognit. Artificial Intelligence* **21** 879–98

[14] Fang W P 2008 Friendly progressive visual secret sharing *Pattern Recognit.* **41** 1410–4

[15] Jena D and Jena S K 2009 A novel visual cryptography scheme *ICACC: Int. Conf. on Advanced Computer Control* pp 207–11

[16] Chen J, Chen T S, Hsu H C and Lin Y H 2009 Using multi-ringed shadow image of visual cryptography to hide more secret messages *Imaging Sci. J.* **57** 101–8

[17] Kobayashi A S 1993 *Handbook on Experimental Mechanics* 2nd edn (Bethel: SEM)

[18] Patorski K and Kujawinska M 1993 *Handbook of the Moiré Fringe Technique* (Amsterdam: Elsevier)
[19] Post D, Han B and Ifju P 1997 *High Sensitivity Moiré: Experimental Analysis for Mechanics and Materials* (Berlin: Springer)
[20] Dai F L and Wang Z Y 1999 Geometric micron moiré *Opt. Laser Eng.* **31** 191–208
[21] Desmedt Y and Van Le T 2000 Moiré cryptography *7th ACM Conf. on Computer and Communications Security* pp 116–24
[22] Lebanon G and Bruckstein A M 2001 A variational approach to moiré pattern synthesis *J. Opt. Soc. Am.* A **18** 1371–81
[23] Lebanon G and Bruckstein A M 2001 On designing moiré patterns *Lect. Notes Comput. Sci.* **2134** 185–201
[24] Munoz-Rodriguez J A and Rodriguez-Vera R 2004 Image encryption based on moiré pattern performed by computational algorithms *Opt. Commun.* **236** 295–301
[25] Ragulskis M, Aleksa A and Saunoriene L 2007 Improved algorithm for image encryption based on stochastic geometric moiré and its application *Opt. Commun.* **273** 370–8
[26] Ragulskis M and Aleksa A 2009 Image hiding based on time-averaging moiré *Opt. Commun.* **282** 2752–9
[27] Ragulskis M and Navickas Z 2007 Hash function construction based on time average moiré *Discrete Contin. Dyn. Syst.* B **8** 1007–20
[28] Watson G N 1995 *A Treatise on the Theory of Bessel Functions* (Cambridge: Cambridge University Press)
[29] Ragulskis M, Saunoriene L and Maskeliunas R 2009 The structure of moiré grating lines and its influence to time-averaged fringes *Exp. Tech.* **33** 60–4
[30] Wetta P, Goutte R and Amiel M 1980 Digital deconvolution of degraded images by a space-invariant motion blur *Signal Process.* **2** 323–38
[31] MacAdam D P 1970 Digital image restoration by constrained deconvolution *J. Opt. Soc. Am.* **6** 1617–27
[32] Navickas Z and Ragulskis M 2007 Representation of time averaged vibrating images in the operator format *J. Vibroeng.* **9** 1–9
[33] Ragulskis M, Sanjuan M and Saunoriene L 2007 Applicability of time average moiré techniques for chaotic oscillations *Phys. Rev.* E **76** 036208